Origins of smooth muscle and evolutionary specializations of the pulmonary mesenchyme in the vertebrate lung

Katharine Goodwin[1‡], Michael A. Palmer[2‡], Bezia Lemma[2], and Celeste M. Nelson[2,3*]

1. Lewis-Sigler Institute for Integrative Genomics, Princeton University, Princeton, NJ 08544, USA
2. Department of Chemical and Biological Engineering, Princeton University, Princeton, NJ 08544, USA
3. Department of Molecular Biology, Princeton University, Princeton, NJ 08544, USA

(‡) These authors contributed equally.

(*) Address correspondence to C.M.N.
303 Hoyt Laboratory, William Street
Princeton, NJ 08544
Tel: 609-258-8851
Fax: 609-258-1247
E-mail: celesten@princeton.edu

Abbreviations: αSMA, α-smooth muscle actin; CK, cytokeratins; *E*, embryonic day; scRNA-seq, single cell RNA sequencing; UMAP, uniform manifold approximation and projection

Summary

Evolution has generated a beautiful diversity of epithelial architectures in the lungs of terrestrial vertebrates, from the tree-like lungs of mammals, to the sac-like lungs of reptiles, to the looped airways of birds. The physical mechanisms that generate pulmonary epithelia of such different shapes are just beginning to be uncovered. Pulmonary smooth muscle plays stage-dependent roles in shaping the epithelium during lung development in the mouse, anole, and chicken. We hypothesized that differences in the timing and spatial patterns of smooth muscle differentiation correspond to distinct patterns of gene expression in the pulmonary mesenchyme. To test this hypothesis and investigate differences in pulmonary smooth muscle patterning across terrestrial vertebrates, we generated scRNA-seq datasets from lungs of mouse, anole, and chicken embryos. These data revealed that smooth muscle regulators are expressed in similar patterns in mouse and anole lungs, in which epithelial branches are sculpted by smooth muscle, but diverge in chicken lungs, in which the epithelium branches in the absence of smooth muscle. Pulmonary smooth muscle differentiates from the lung mesenchyme in mouse and anole. Surprisingly, however, bioinformatic and experimental evidence suggest that pulmonary smooth muscle is derived from vascular smooth muscle in chicken. Furthermore, our data revealed differences in the timing and extent of smooth muscle innervation across species. These findings highlight how terrestrial vertebrates have evolutionarily repurposed similar morphogenetic motifs to build lungs that suit their energetic needs.

Keywords

morphodynamics; mechanobiology; mechanical stress

Introduction

Vertebrates from different clades have evolved unique solutions to the problem of gas exchange. The lungs of terrestrial vertebrates are characterized by diverse anatomies and mechanisms for aeration, which may reflect the energetic demands of their respective lifestyles[1]. Mammals have a bronchoalveolar lung, which consists of a complex, tree-like arrangement of terminally branched airways that culminate in blind-ended gas-exchange surfaces, the alveoli[2]. Of fully terrestrial vertebrates, non-avian reptiles have the simplest lungs, which in many cases consist of a single hollow chamber lined by an epithelial sheet that is only rudimentarily corrugated to form faveoli, which slightly increase the surface area available for gas exchange[3]. Avian lungs contain a continuous, closed circuit of airways, interwoven in the gas-exchange regions with the surrounding vasculature. This parabronchial architecture enables unidirectional airflow, which is more efficient than the tidal, bidirectional flow necessitated by a terminally branched lung[4]. In the bird, air is pushed through the lung by the expansion and contraction of air sacs that act as bellows to force air through the rigid gas-exchange air conduits[4]. Despite these differences in epithelial architecture, the lungs of terrestrial vertebrates contain conserved cell types: the airway epithelium itself, the surrounding pulmonary mesenchyme, endothelial cells that form vascular networks and, finally, a mesothelium that encapsulates the organ.

To generate the final architecture of a given organ, the embryos of different species may use different cellular mechanisms, cell types, or a combination thereof. For example, intestinal morphogenesis in the chicken embryo involves the sequential differentiation of three smooth muscle layers that compress the epithelium to generate ridges, zigzags, and then finally villi[5]. The mouse intestinal epithelium develops into a similar final morphology, but its villi are not produced in the same stepwise manner; instead, mouse intestinal villi arise from an initially flat epithelial surface in response to spatial signals from the underlying mesenchyme[6]. Smooth muscle, derived from the pulmonary mesenchyme, also wraps the airway epithelium of vertebrate lungs, where it is believed to have first evolved as a mechanism for exhalation[1,7]. However, increasing evidence points to an additional role for smooth muscle in regulating embryonic lung development.

In the embryonic mouse lung, for example, smooth muscle wraps around the proximal airways beginning at the earliest stages of epithelial branching morphogenesis [embryonic day (*E*) 11]. As branching proceeds, smooth muscle differentiates in a proximal-to-distal (cranial-to-caudal) wave in response to sonic hedgehog (Shh) secreted by the airway epithelium. The pattern of smooth muscle differentiation guides both lateral branching and terminal bifurcations by exerting physical forces that either shape the growing airway epithelium into lateral branches or specify cleft sites[8,9]. Similar patterns of smooth muscle differentiation have been observed during human lung development[10]. In the embryonic lung of the brown anole lizard, smooth muscle forms a contractile meshwork around a balloon-like pulmonary epithelium, inducing the epithelium to form corrugations that later become the faveolar gas-exchange surface[11]. A similar pattern of smooth muscle has been observed in developing frog lungs[12], suggesting that this physical mechanism of morphogenesis might be conserved amongst lungs with simple architectures.

Surprisingly, smooth muscle is absent during the early stages of epithelial branching in the embryonic bird lung and instead differentiates at late stages of development (~*E*7 in the chicken). In the absence of smooth muscle, branching of the embryonic chicken airway epithelium (*E*4 onwards) is driven by apical constriction of the epithelial cells themselves[13,14]. Apical constriction also drives airway branching in the

lungs of other species of birds[15]. Nonetheless, smooth muscle might play a role in guiding the airways towards each other during the extensive process of airway fusion, called anastomosis, that occurs later in development (*E*10-*E*13)[16]. Patterns of airway smooth muscle differentiation also presage morphogenesis of the atria, which are small epithelial branches that give rise to the air capillaries that interweave with the surrounding gas-exchange vasculature in the bird lung[16]. Pulmonary smooth muscle differentiation is thus a common feature of lung morphogenesis in terrestrial vertebrates, but the molecular pathways that control its distinct timing and patterns remain unclear.

Here, we took advantage of these known differences in the timing and patterning of smooth muscle differentiation to uncover the gene-expression programs that correlate with lung anatomy across species. Specifically, we examined the smooth muscle transcriptome at the single-cell level during lung morphogenesis in three model systems: the mouse (*Mus musculus*), the brown anole lizard (*Anolis sagrei*), and the domestic chicken (*Gallus gallus*). We generated single-cell RNA-sequencing (scRNA-seq) datasets of whole lungs isolated at different stages of development in each species. Using these datasets, we compared the transcriptional signatures of undifferentiated mesenchymal and smooth muscle cells as a function of time across species. We found that the pulmonary mesenchyme of chicken embryos lacks widespread expression of Shh receptors in the early stages of lung development, consistent with the absence of airway smooth muscle at these stages. Activating Shh signaling in chicken lung explants cultured *ex vivo*, which enhances pulmonary smooth muscle differentiation from the sub-epithelial mesenchyme in mouse and anole, induces the ingression of distal mesothelial cells that express the smooth muscle marker α-smooth muscle actin (αSMA). Immunofluorescence analysis of a developmental time-course suggests that these cells shape the distal air sacs of the chicken respiratory system. Comparing the transcriptomes of smooth muscle cells from our datasets to those of airway, vascular, lymphatic, and skeletal muscle cells from published datasets reveals that the chicken airway smooth muscle is surprisingly similar to pulmonary vascular smooth muscle in mouse embryos. Consistently, immunofluorescence analysis revealed a tight spatial correlation between vascular smooth muscle and the first smooth muscle cells wrapping the major airways in the embryonic chicken lung. Finally, we carried out integrated computational analyses to identify mesenchymal populations common to or unique to each species. This analysis revealed a population of cells that supports innervation that is enriched in the anole, which correlates with the development of a dense network of neurons that innervates the highly contractile smooth muscle mesh in the reptilian lung. In conclusion, our findings shed new light on the mechanistic origins of the divergence of lung architectures that arose during the evolution of terrestrial vertebrates.

Results

Generation of scRNA-seq datasets from the lungs of representative terrestrial vertebrates

To gain an evolutionary perspective on the signaling pathways that control the pattern and dynamics of pulmonary smooth muscle differentiation across mammals, reptiles, and birds, we generated scRNA-seq datasets from the lungs of three species: mouse (*Mus musculus*), brown anole (*Anolis sagrei*), and chicken (*Gallus gallus*). For the mouse, we selected *E*12.5 as a timepoint during which the epithelium is actively undergoing branching morphogenesis concomitant with a proximal-to-distal wave of smooth muscle differentiation (**Fig. 1A**). Since airway smooth muscle differentiates continuously in the embryonic mouse lung, this developmental timepoint contains smooth muscle cells at all stages of differentiation from the

pulmonary mesenchyme[17]. We focused on the left lobe of the mouse lung to avoid any complications due to differences in timing of morphogenesis across the four lobes of the right lung. For the anole, we selected *E*5 and *E*6, given that smooth muscle differentiates essentially simultaneously around the entire lung epithelium[11]. Capturing these two days of development allows us to compare the transcriptomes of pulmonary mesenchymal cells before (*E*5) and during (*E*6) smooth muscle differentiation (**Fig. 1B**). For the chicken, we selected a wider range of developmental stages, since the dynamics of smooth muscle differentiation are extended in avian lungs as compared to those of mammals and reptiles. We generated datasets at *E*4 and *E*5 (HH 22-23 and HH25-26), which correspond to the early stages of epithelial branching morphogenesis that occurs in the absence of smooth muscle (**Fig. 1C**). To capture the early stages of airway smooth muscle differentiation, we selected *E*8 (HH33), and to capture the later stages of smooth muscle differentiation that accompany airway anastomosis, we selected *E*12 (HH37; **Fig. 1C**).

For each dataset, we performed clustering to identify mesenchymal cells (including smooth muscle) and then computationally isolated these populations from the other cell types (e.g. epithelium, vascular endothelium). We also corrected each dataset for cell-cycle stage, and then generated uniform manifold approximation and projection (UMAP) plots to visualize the mesenchymal clusters. The mesenchyme appears as a continuous population of cells in all datasets, without any obvious isolated clusters (**Fig. 1D**), in line with previous work examining single-cell transcriptomes of early embryonic organs[17,18]. These data suggest that the embryonic pulmonary mesenchyme of all three species contains a continuum of cell states from undifferentiated progenitors to mature smooth muscle. To confirm this conclusion, we overlaid the expression of the smooth muscle marker α-smooth muscle actin (*Acta2*) on each UMAP (**Fig. 1E**). Clear gradients of *Acta2* expression can be observed in the mouse *E*12 and anole *E*6 datasets, reaching the highest levels in cluster 4 and cluster 1, respectively. As expected, *Acta2* expression is less prominent at *E*5 in the anole and almost absent at *E*4 and *E*5, but detectable at *E*8 and *E*12, in the chicken. The small population of cells in the chicken *E*5 dataset that express *Acta2* and *Hhip* correspond to vascular smooth muscle (**Fig. 1C**). These scRNA-seq datasets are therefore in agreement with known trends in pulmonary smooth muscle differentiation across developmental time, and enable the study of mesenchymal patterning across species.

Expression of genes associated with the hedgehog signaling pathway in the pulmonary mesenchyme

The embryonic mouse airway epithelium expresses sonic hedgehog (*Shh*), which induces the surrounding mesenchyme to differentiate into airway smooth muscle[19]. In both mouse and anole embryonic lungs, we previously found that stimulating or inhibiting Shh signaling increases or decreases smooth muscle differentiation, respectively[8,11]. We therefore analyzed the expression of the Shh receptor Patched1 (*Ptch1*) and the Shh-target-gene hedgehog interacting protein (*Hhip*) in mesenchymal cells of mouse, anole, and chicken lungs.

As expected, *Ptch1* expression is broadly distributed throughout the mesenchyme of the mouse and anole datasets, suggesting that a large cohort of pulmonary mesenchymal cells is capable of binding to the Shh ligand (**Fig. 1F**). On the other hand, *Hhip*, which is activated by Shh signaling, is predominantly expressed in *Acta2*-positive mesenchymal cells (**Fig. 1G**). This pattern is consistent with the fact that transduction of the Shh signal induces smooth muscle differentiation. Surprisingly, both *Ptch1* and *Hhip* are only sparsely detected in the mesenchyme of the embryonic chicken lung, even at later stages when *Acta2* expression is more widespread.

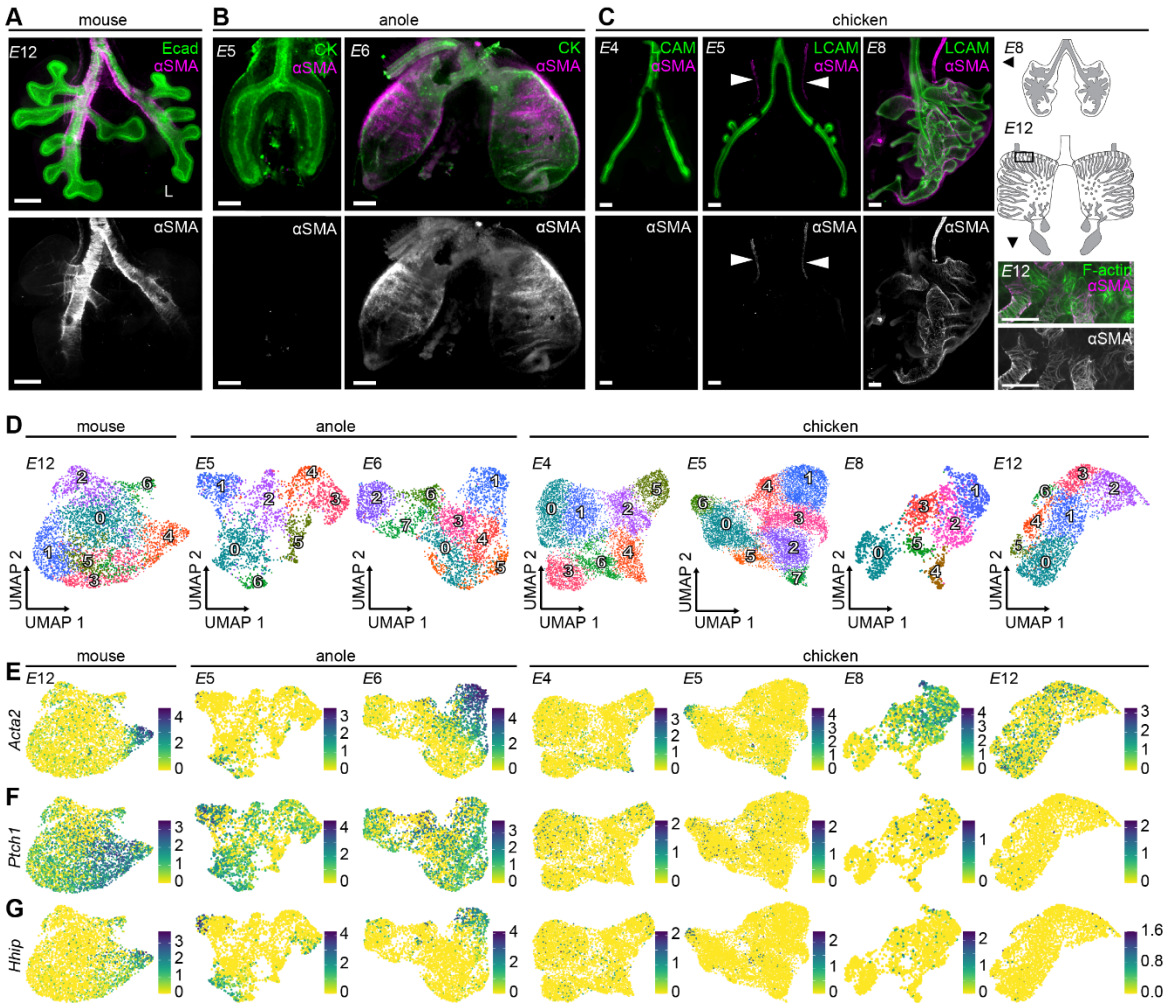

Figure 1: scRNA-seq analysis of embryonic mouse, anole, and chicken lungs. (**A**) Confocal images of *E*12 mouse lungs immunostained for Ecad and αSMA. "L" indicates left lobe. (**B**) Confocal images of *E*5 and *E*6 anole lungs immunostained for cytokeratins (CK) and αSMA. (**C**) Confocal images of *E*4, *E*5, *E*8, and *E*12 chicken lungs immunostained for either LCAM or F-actin and αSMA. Whole lungs are shown for *E*4 and *E*5, one lobe is shown for *E*8, and a zoomed-in view of anastomosing airways is shown for *E*12 (as indicated in the accompanying schematics). Arrowheads show vascular smooth muscle. Scale bars represent 100 µm. (**D**) UMAPs of mesenchymal cells from *E*12 mouse lungs, *E*5 and *E*6 anole lungs, and *E*4, *E*5, *E*8, and *E*12 chicken lungs, color-coded based on automatically defined clusters. (**E-G**) Expression of *Acta2*, *Ptch1*, and *Hhip* in the mesenchymal clusters reveals overlap of *Acta2* and *Hhip* in mouse and anole, and relative absence of *Ptch1* and *Hhip* in chicken.

We then examined other components of the Shh pathway. *Shh* is not detected in any mesenchymal dataset (**Supplementary Fig. 1A**), as expected since this ligand is known to be expressed by the lung epithelium. *Ptch2* shows similar expression patterns (and lack of expression in chicken) as *Ptch1* (**Supplementary Fig. 1B**). Smoothened (*Smo*) is sparsely detected in the anole and chicken at early stages of lung development but is present throughout the mesenchyme of the mouse lung (**Supplementary Fig. 1C**). The Gli transcription factors are detected in each dataset, with more cells expressing *Gli2* and *Gli3* than

Gli1 (**Supplementary Fig. 1D-F**). Suppressor of fused (*Sufu*) is detected throughout the lung mesenchyme in mouse and anole, but not chicken (**Supplementary Fig. 1G**).

We also examined patterns of *Fgf10* expression, given the role of this growth factor in mouse lung development[20,21]. A small number of *Fgf10*-expressing cells is present in the mouse dataset and at early stages of chicken lung development. The number of *Fgf10*-expressing cells increases at later stages in the chicken, whereas neither stage of anole lung development contains more than a handful of *Fgf10*-expressing cells (**Supplementary Fig. 1H**). No other FGF ligands are detected at appreciable levels in any of the datasets (not shown). The FGF receptors *Fgfr1* and *Fgfr2* both show relatively homogeneous expression patterns in all datasets, but with a slight skew towards *Fgfr1* in the mouse and *Fgfr2* in the anole (**Supplementary Fig. 1I-J**). *Fgfr3* is largely absent from the mouse and completely absent from the anole lung mesenchyme but is detected at very high levels and with clear cluster-specific differences at all stages of chicken lung development (**Supplementary Fig. 1K**). *Fgfr3* has previously been shown to be enriched in the sub-epithelial mesenchyme of the chicken lung by *in situ* hybridization[22], and the *Fgfr3*-expressing clusters in our datasets may correspond to this mesenchymal compartment. *Fgfr4* is largely absent from mouse, detected at low levels in chicken, and at slightly higher levels in anole (**Supplementary Fig. 1L**). These gene-expression patterns suggest that FGF ligands and receptors may be deployed in slightly different ways across these three species, which is unsurprising given the known discrepancies between FGF signaling in mouse and human lungs[23].

These results suggest a divergence in the signaling pathways responsible for pulmonary smooth muscle differentiation, with Shh signaling serving as an activator in the lungs of mammals and reptiles, but not birds. This divergence may be related to the difference in the stage at which this tissue appears in birds, which acquire smooth muscle later in lung development as compared to mammals and reptiles, which acquire smooth muscle early.

Shh signaling elicits distinct patterns of smooth muscle differentiation in mouse, anole, and chicken
Based on differential expression of components of the Shh signaling pathway in chicken compared to mouse and anole, we hypothesized that the mesenchyme of the embryonic chicken lung may not be responsive to Shh produced by the airway epithelium. We tested this hypothesis by examining whether the pulmonary mesenchyme of the embryonic chicken lung could differentiate into smooth muscle in response to exogenous activation of Shh signaling. We treated *E*5 chicken lung explants with smoothened agonist (SAG), which activates the Shh signaling pathway downstream of Patched receptors[24]. Smooth muscle was absent from the epithelium of both vehicle- and SAG-treated explants after 24 hours of culture (**Fig. 2A**). Instead, we observed a cluster of αSMA-expressing cells that appeared to originate from the lateral mesothelium distal to the actively branching region of the lung and then migrate into the mesenchyme towards the epithelium (**Fig. 2A**). This αSMA-expressing cluster was located in the same position in vehicle- and SAG-treated explants (**Fig. 2B-C**). However, the cluster was wider in SAG-treated explants (**Fig. 2B, D**), suggesting that activating Shh leads to increased differentiation and/or migration of αSMA-expressing cells from this distinct location in the distal mesothelium.

We tested the validity of this conclusion using fluorescent labeling experiments (**Supplementary Fig. 2**). Prior to culturing, lungs were briefly incubated with DiI, which labeled mesothelial cells on the surface of the explant but which was restricted from cells deeper within the organ. After 24 hours of culture with or

without SAG, DiI-labeled cells were exclusively located at the surface of mouse and anole lungs (**Fig. 2E-F, Supplementary Fig. 2A-B**). In the embryonic chicken lung however, DiI-labeled cells were present within the distal mesenchyme, in the same location as the αSMA$^+$ cluster, after 24 hours of culture with or without SAG (**Fig 2G, Supplementary Fig. 2C**). The extent of labeling was greater in SAG-treated lungs (**Fig. 2H**), indicating that the invasion of these cells is a normal process that is enhanced by ectopic Shh signaling. DiI-labeled cells were observed at a greater distance into the mesenchyme than αSMA$^+$ cells, suggesting fairly widespread migration of mesothelial cells into the pulmonary mesenchyme. The differences in invasion distance can also be attributed to sample clearing, which shrinks lungs and therefore leads to smaller distances measured in fixed and cleared samples (**Fig. 2D**) compared to live explants (**Fig. 2H**). These data suggest that Shh does not induce the differentiation of pulmonary mesenchymal cells into airway smooth muscle in the avian lung. Instead, we identify a Shh-responsive population of mesothelial cells that invade the pulmonary mesenchyme adjacent to the distal lung epithelium and express markers of smooth muscle.

To better understand how mesothelial cells could differentiate into αSMA-expressing cells in the embryonic chicken lung, we examined the expression of Shh-pathway genes in the mesothelium. At *E*5, mesothelial cells (marked by *Krt7* expression) in the chicken lung express relatively low levels of *Ptch1*, *Ptch2*, *Gli1*, *Gli3*, *Smo*, and *Sufu* (**Supplementary Fig. 2D**). Mesothelial cells do, however, express high levels of *Gli2*, which may enable these cells to respond to treatment with SAG. Different signaling pathways may activate the expression of αSMA in mesothelial cells, or the mesothelium may increase its expression of Shh-pathway components at later stages of development. Alternatively, the population of mesothelial cells that are responsive to exogeneous activation of Shh signaling and that invade the mesenchyme may be below the threshold of detection in our scRNA-seq dataset. Spatial gene-expression analysis using fluorescence in situ hybridization or spatial transcriptomics may be required to determine if there is highly localized expression of Shh-pathway components in the distal mesothelium.

Although its morphogenesis has not been well characterized, the distal epithelium of the bird lung is thought to give rise to the smooth muscle-wrapped air sacs that will eventually ventilate the rigid airways after hatching[4] (**Fig. 2I**). We therefore examined patterns of smooth muscle around the distal epithelium at different stages of development. The distal epithelium lengthens from *E*6 to *E*7 (**Fig. 2J**) and forms a lateral branch by *E*8 (**Fig. 2K-L**). Similar to the early stages of lung development, this lateral branch forms prior to the appearance of smooth muscle (**Fig. 2J-K**), but the branch point becomes increasingly wrapped by smooth muscle over time (**Fig. 2M**). The morphology of the branch point also gradually changes over time, taking on a tighter shape with increased smooth muscle wrapping (**Fig. 2M-N**). This pattern of coverage is somewhat reminiscent of that observed at the neck of epithelial bifurcations in the embryonic mouse lung (**Fig. 2O**). This similarity in morphology suggests that sculpting forces from smooth muscle may also refine this branch point in the avian lung. Therefore, while branching of the avian airways occurs largely in the absence of airway smooth muscle, the morphology of the avian air sac epithelium is refined concomitant with smooth muscle wrapping. The mechanical role for smooth muscle observed in development of the mouse and anole lungs may be conserved in the air sacs of the chicken lung.

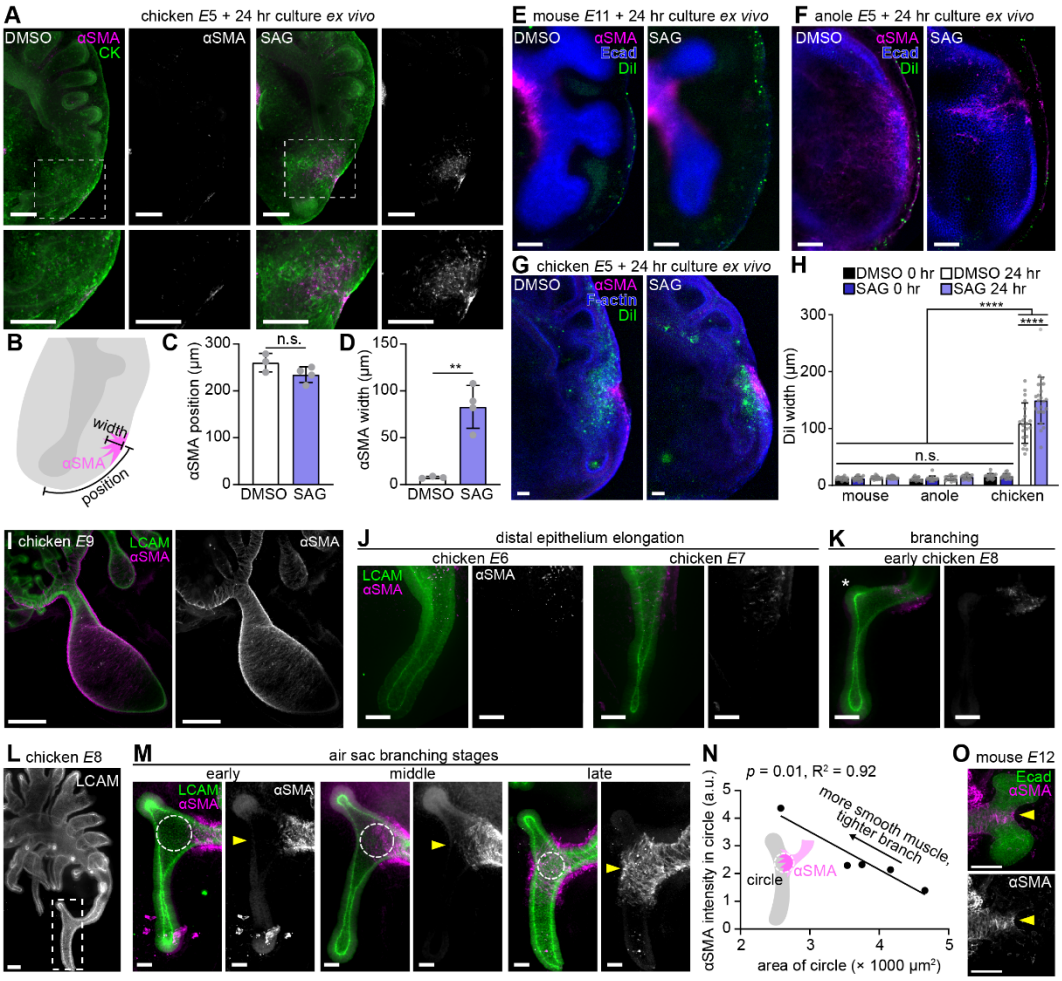

Figure 2: A possible mesothelial origin of air-sac smooth muscle cells in the chicken. (**A**) Chicken lungs isolated at *E*5 and cultured for 24 hours *ex vivo* in the presence of DMSO or SAG (1 µg/ml) prior to immunostaining for CK and αSMA. Box indicates zoomed-in region shown beneath. (**B**) Schematic illustrating how width (from the surface of the organ) and position (from the distal tip of the organ) of clusters of αSMA$^+$ cell were measured. (**C-D**) Width and position of the cluster of αSMA$^+$ cells in *E*5 chicken lungs treated with DMSO or SAG for 24 hours. (**E-G**) Mouse lungs isolated at *E*11, anole lung isolated at *E*5, or chicken lungs isolated at *E*5 incubated with DiI to label the mesothelial surface of the lung, and then cultured for 24 hours *ex vivo* in the presence of DMSO or SAG (1 µg/ml) prior to immunostaining for Ecad or F-actin and αSMA. (**H**) Quantification of the width of the cluster of DiI-labeled cells (measured from the surface of the organ) before and after culture in the presence of DMSO or SAG in all three species. (**I**) Air sacs of *E*9 chicken lungs immunostained for LCAM and αSMA. (**J**) Distal part of *E*6 and *E*7 chicken lungs immunostained for LCAM and αSMA showing elongation of epithelium in the absence of smooth muscle wrapping. (**K**) Distal part of an *E*8 chicken lung immunostained for LCAM and αSMA showing the formation of a lateral branch in the absence of smooth muscle wrapping. (**L-M**) *E*8 chicken lungs at various stages of air sac morphogenesis immunostained for LCAM and αSMA. Dashed white box in (L) highlights zoomed-in regions in (M), which show distal epithelium that gives rise to air sacs. Yellow arrowheads indicate smooth muscle in epithelial cleft. (**N**) Quantification of branch morphology (defined as the area of the largest circle that fits within the branch point, indicated in the schematic) and smooth muscle wrapping (defined as the intensity of αSMA staining within the circle) in *E*8 chicken lungs at different stages of air sac morphogenesis. Shown are results of simple linear regression and associated *p* and R^2 values. (**O**) *E*12 mouse lung immunostained for Ecad and αSMA. Yellow arrowheads indicate smooth muscle in epithelial cleft. Scale bars represent 50 µm. ** denotes $p < 0.01$, **** $p < 0.0001$, n.s. means not significant.

Airway smooth muscle in the chicken lung resembles and appears to originate from vascular smooth muscle

Based on their divergent gene-expression profiles, we hypothesized that the pulmonary smooth muscle cells of the chicken might represent a fundamentally different cell type from those of the mouse or anole. We therefore compared pulmonary smooth muscle gene expression in mouse, anole, and chicken to that of several different contractile cell types by taking advantage of published datasets that were generated from a variety of organs in the mouse (**Supplementary Figure 3**). We included airway smooth muscle, vascular smooth muscle, myofibroblasts, and pericytes from embryonic and postnatal mouse lungs[25], myocardial cells from embryonic mouse hearts[26], lymphatic smooth muscle cells from adult mice[27], and muscle stem cells from quadricep and diaphragm skeletal muscles from adult mice[28].

Pulmonary smooth muscle cells from our mouse *E*12 dataset (cluster 4) are most similar to airway smooth muscle cells of the published dataset acquired at the same stage of lung development (**Fig. 3A**). These cells (cluster 4) are less similar to those from published datasets acquired at later stages of development, perhaps because the *E*12 mouse lung contains immature smooth muscle cells that are transcriptionally distinct from mature smooth muscle[17]. We also observed some correlation between *E*12 pulmonary smooth muscle and early-stage vascular smooth muscle, lymphatic smooth muscle, and myocardial cells. The lowest correlations are with postnatal vascular smooth muscle, pericytes, and skeletal muscle stem cells.

Pulmonary smooth muscle from the anole (cluster 1) is most similar to the two airway smooth muscle clusters from *E*12.5 mouse lungs and least similar to vascular smooth muscle from *E*17.5 mouse lungs (**Fig. 3B**). Correlations with all other datasets are similarly low, suggesting that pulmonary smooth muscle in the anole is transcriptionally similar to airway smooth muscle in the mouse. Surprisingly, pulmonary smooth muscle from the chicken (cluster 1) is most similar to vascular smooth muscle from *E*15.5 mouse lungs, and by a large margin (**Fig. 3C**). Moderate correlations are observed with airway smooth muscle from *E*12.5 mouse lungs and myofibroblasts and pericytes from *P*3 mouse lungs. These data are consistent with our conclusion that pulmonary smooth muscle in the chicken is fundamentally different from that in the mouse and anole.

This observed correlation prompted us to examine patterns of vascular smooth muscle in the lungs of each species. At the stages from which our scRNA-seq datasets were generated, mouse and anole have very small amounts of vascular smooth muscle lining the large blood vessels that run parallel to the upper airways (**Fig. 3D-E**). The amount of pulmonary smooth muscle thus dwarfs that of vascular smooth muscle at these stages of development. Conversely, smooth muscle in *E*5 chicken lungs is exclusively vascular and can be detected wrapping the pulmonary artery that runs alongside the airways, including near the first domain branches of the airway epithelium (**Fig. 3F**). By *E*6, a halo of αSMA^+ cells emanates from this vascular smooth muscle layer, and sparse αSMA^+ cells are detected throughout the mesenchyme between blood vessels and epithelial branches (**Fig. 3G**). This pattern of αSMA^+ cells dispersed throughout the mesenchyme (and not directly adjacent to endothelial or epithelial cells) is never observed in mouse or anole lungs and appears to reflect the migration of smooth muscle cells through the mesenchyme. In addition, small numbers of αSMA^+ cells appear to wrap some epithelial branches in the vicinity of the pulmonary artery (**Fig. 3H**). Based on these observations, we propose that airway smooth muscle in the chicken lung may be derived from vascular smooth muscle. Whether these vascular smooth

muscle cells differentiate from the surrounding mesenchyme or migrate into the lung from an external source is unclear. These unanswered questions will require novel labeling and/or lineage-tracing strategies for chicken embryos, along with approaches for live-imaging of vascular development during organogenesis.

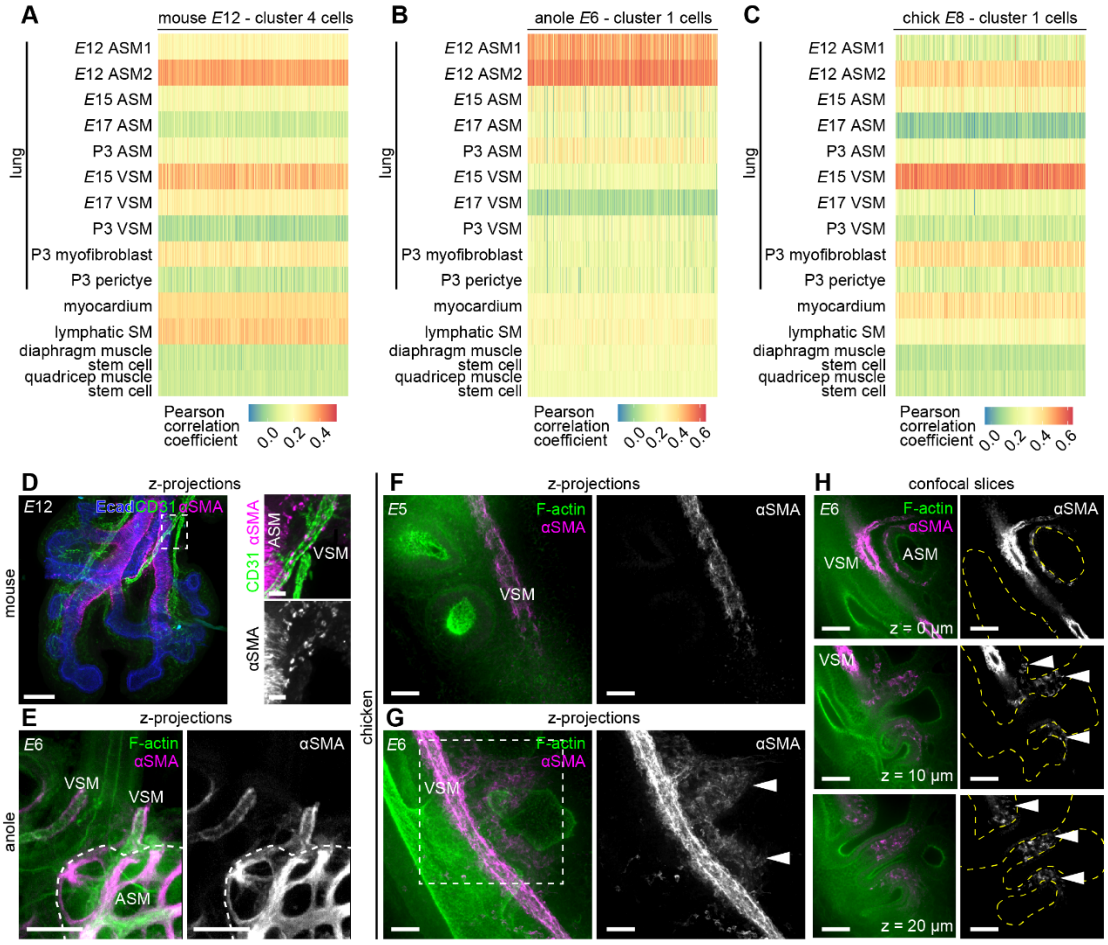

Figure 3: Chicken airway smooth muscle is similar to, and appears to derive from, pulmonary vascular smooth muscle. (**A-C**) Pearson correlation analysis comparing gene expression in smooth muscle cells from each species to that of muscle cells from various mouse organs. (**D**) Confocal images of *E*12 mouse lungs immunostained for Ecad, CD31 (to label blood vessels), and αSMA. Zoomed-in images correspond to region in dashed white box. Airway smooth muscle (ASM) and vascular smooth muscle (VSM) are indicated. (**E**) Confocal images of the caudal portion of an *E*6 anole lung immunostained for F-actin and αSMA. Airway smooth muscle (ASM, and dashed white line) and vascular smooth muscle (VSM) are indicated. (**F**) Confocal images of *E*5 chicken lungs immunostained for F-actin and αSMA. (**G-H**) Confocal images of *E*6 chicken lungs immunostained for F-actin and αSMA. Confocal z-projections and single slices at different z-depths are shown. Yellow dashed line outlines epithelium. Arrowheads indicate αSMA$^+$ cells that appear to be migrating through the mesenchyme between the blood vessel and the airway epithelium. Scale bars represent 25 µm.

Integration of datasets reveals mesenchymal populations unique to each species
To expand our analysis to mesenchymal cell types other than smooth muscle, we integrated our mouse *E*12, anole *E*6, and chicken *E*8 datasets using Seurat (**Fig. 4A**). The datasets of each species showed significant overlap, consistent with successful integration (**Fig. 4B**). This analysis also revealed clusters of cells that are unique to or enriched in each species (**Fig. 4B-C**).

Based on *Acta2* expression and gene ontology analysis, we determined that cluster 6 of the integrated dataset represents smooth muscle (**Fig. 4D**). Cluster 6 includes cells from all three species, but relatively more from the anole (**Fig. 4A-E**). This apparent enrichment could be due to the simultaneous differentiation of smooth muscle all around the lung epithelium in this species, which would presumably lead to a relatively high proportion of smooth muscle cells in the pulmonary mesenchyme of anole lungs. Based on *Ptch1* expression, we determined that clusters 0 to 3 represent undifferentiated mesenchyme and possible smooth muscle precursors (**Fig. 4D**). Gene ontology analysis suggested that clusters 0, 2, and 3 are primarily characterized by the expression of cell-cycle genes, as would be expected in progenitor cells (**Fig. 4E**). Additionally, we observed that these clusters are enriched for cells from the mouse (**Fig. 4C**), leading us to hypothesize that the mouse pulmonary mesenchyme is more proliferative than that of the anole or chicken. To test this hypothesis, we carried out EdU incorporation analysis and quantified the number of EdU^+ cells in the mesenchyme as an indicator of proliferation. We found that the pulmonary mesenchyme is twice as proliferative in the mouse as in the anole or the chicken (**Fig. 4F-G**), consistent with our hypothesis based on scRNA-seq analysis. Cluster 1, which primarily contains cells from the anole and chicken and lacks cells from the mouse, might contain a population of smooth muscle progenitors that is less proliferative than that in the mouse. Consistently, cells of this cluster express markers of early smooth muscle, including *Bmp4* and *Sdc2*[17], at similar levels to clusters 0, 2, and 3 (**Fig. 4H-K**).

Our analysis also identified clusters of mesenchymal cells that are enriched in anole lungs (clusters 4 and 7) (**Fig. 4B-C**). Cluster 4 is enriched for genes involved in limb morphogenesis, but closer inspection revealed that these genes (e.g., *Sox9,* **Fig. 4D**) are also expressed by cartilage precursors of the lung. The upper airways of the mature mouse lung are surrounded by half-rings of smooth muscle and cartilage, and $Sox9^+$ cartilage precursors are present at *E*12.5 (**Fig. 4L**). $Sox9^+$ cells are present around the entire circumference of the upper airways in *E*8 chicken lungs, which lack smooth muscle wrapping (**Fig. 4M**). Our mouse *E*12 scRNA-seq dataset was generated from left lobes that were isolated away from the upper airways (schematic in **Fig. 4L**). Similarly, our chicken *E*8 scRNA-seq dataset was generated from lungs dissected away from the upper airways (schematic in **Fig. 4M**). These dissections resulted in small proportions of $Sox9^+$ mouse and chicken cells in cluster 4 of the integrated analysis. Conversely, our anole *E*6 dataset included cells of the upper airways (schematic in **Fig. 4N**). Immunofluorescence analysis revealed that $Sox9^+$ cells wrap around the entire circumference of the upper airways in the anole, which lack smooth muscle wrapping (**Fig. 4N**), similar to the chicken. This early pattern of $Sox9^+$ cells results in the formation of cartilage rings that completely encircle the upper airways at later stages of development of the embryonic anole lung (**Fig. 4O**). The cartilage that fully or partially surrounds the upper airways in these species acts as a rigid support to keep the airways open and prevent collapse[29,30]. The various patterns of cartilage and smooth muscle around the upper airways are thought to be related to neck flexibility and associated requirements pertaining to feeding: mammals retain the ancestral tracheal and esophageal positioning dorso-ventrally to one another along the lateral midline – incomplete cartilage

rings permit the esophagus to expand during feeding[31]. In contrast, birds are able to achieve significantly greater neck flexibility by having the esophagus and trachea detached and misaligned laterally, allowing the trachea to be less flexible and fully wrapped by cartilage rings[32]. The presence of Sox9^{+} cells in the anole dataset and their pattern revealed by immunofluorescence suggest that the development and function of reptilian cartilage rings may parallel that of birds.

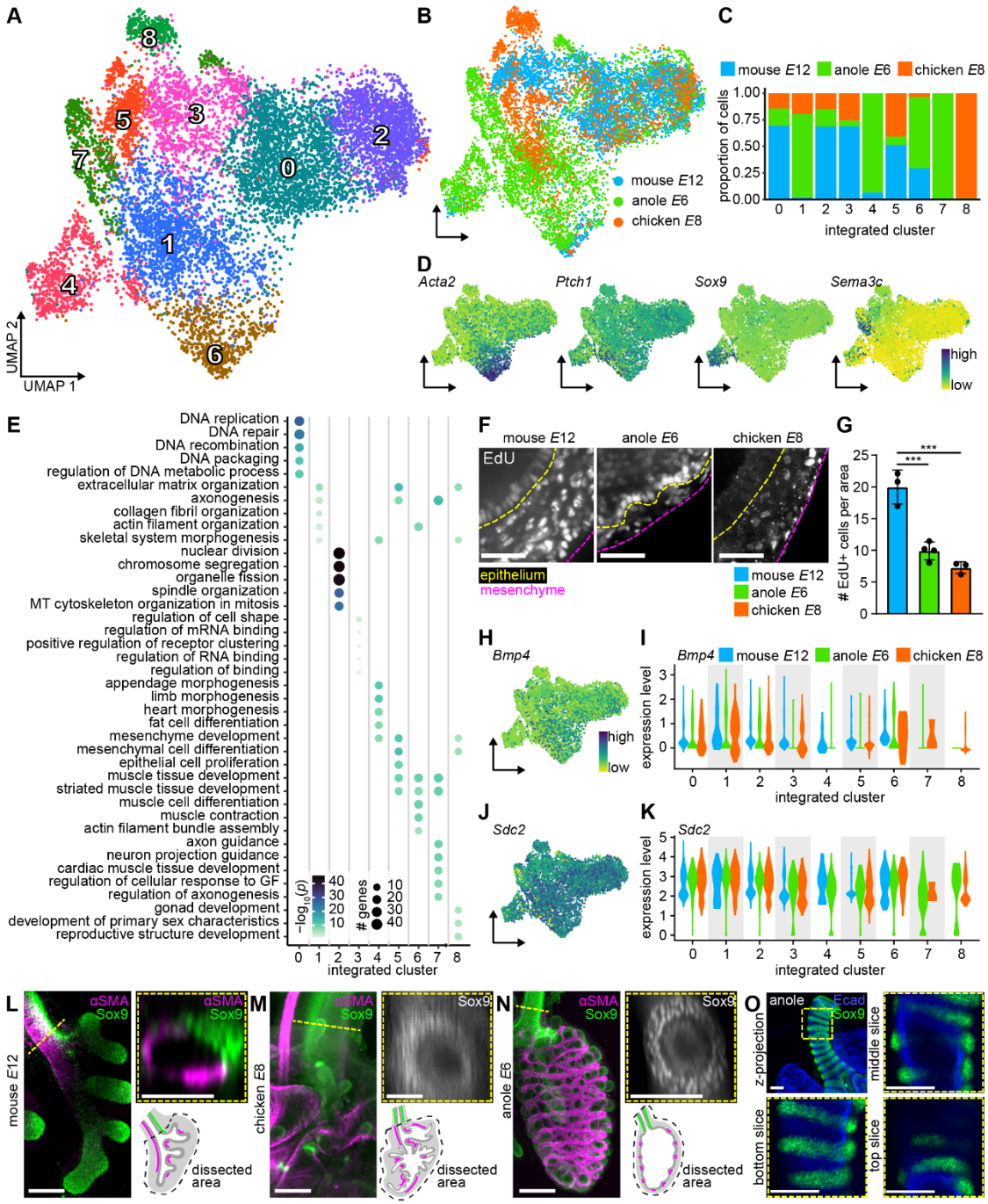

Figure 4: Integrated scRNA-seq analysis reveals features of the pulmonary mesenchyme specific to each species. (**A**) UMAP of integrated mouse *E*12, anole *E*6, and chicken *E*8 mesenchymal cell datasets color-coded by cluster. (**B**) UMAP from (A) color-coded by species. (**C**) Proportion of each cluster

represented by each species. (**D**) UMAP from (A) color-coded according to the expression of *Acta2*, *Ptch1*, *Sox9*, or *Sema3c*. (**E**) Gene ontology enrichment analysis of markers of each cluster. (**F**) EdU incorporation in *E*12 mouse, *E*6 anole, and *E*8 chicken lungs. Epithelium and mesenchyme are indicated. (**G**) Quantification of EdU^+ cells in the mesenchyme per 1000 μm^2. (**H-K**) UMAPs and violin plots showing cluster- and species-specific expression levels of the early smooth muscle markers *Bmp4* and *Sdc2*. (**L-N**) *E*12 mouse, *E*6 anole, and *E*8 chicken lungs immunostained for Sox9 and αSMA and schematic of smooth muscle, cartilage rings, and area dissected for scRNA-seq. Shown are confocal z-projections and optical cross-sections through the upper airways (indicated by yellow dashed line). Scale bars indicate 100 µm. (**O**) Confocal projections and single slices at different cross-sections of the trachea of an *E*10 embryonic anole lung immunostained for Sox9 and phalloidin (F-actin), showing full cartilage rings. *** indicates $p < 0.001$. Scale bars indicate 50 µm.

The mesenchyme supports different levels of innervation in each species

Cluster 7 of our integrated dataset is enriched for genes involved in axonogenesis, including semaphorin 3c (*Sema3c*) (**Fig. 4D-E**). Immunofluorescence analysis for the cluster marker Sema3c and the neuronal marker Piezo1 revealed $Sema3c^+$ mesenchymal cells in close proximity to neurons in the lungs of all three species (**Fig. 5A-C**). This observation led us to hypothesize that innervation is supported by distinct populations of pulmonary mesenchymal cells, which are enriched in the anole. If this hypothesis were correct, we would predict to find more neurons in the lung of the anole than in that of the mouse or chicken.

To test this hypothesis, we visualized neurons in the lungs of each species using wholemount immunofluorescence analysis for Piezo1 (**Fig. 5D-F**). In *E*12 mouse lungs, Piezo1 labeled the vagus nerve and a few sparse nerves along the upper airways (**Fig. 5D**). We observed a similar pattern in *E*8 chicken lungs (**Fig. 5F**). In contrast, staining for Piezo1 in *E*6 anole lungs revealed an intricate network of nerves surrounding the epithelium that is far more extensive than those in the mouse or chicken (**Fig. 5E**). We quantified the extent of innervation by measuring the total length of all $Piezo1^+$ nerves, normalized to the area of the epithelium, and found 50% higher levels in anole lungs compared to mouse or chicken (**Fig. 5G**).

This more extensive innervation may enable the dramatic contractions of the pulmonary smooth muscle in the anole. Mouse and chicken lungs exhibit infrequent spontaneous contractions of smooth muscle that rapidly constrict the upper airways (**Fig. 5H, J, Supplementary Movies 1, 3**). Anole lungs contract far more dramatically (**Fig. 5I, Supplementary Movie 2**). The frequency of contractions is significantly higher in the anole (**Fig. 5K**), as is the magnitude of contractions, measured as the change in airway width (**Fig. 5L**). More extensive innervation of the smooth muscle mesh may enable the stronger and more frequent spontaneous contractions in the anole lung. Our integrated scRNA-seq analysis has therefore revealed a specialization of the reptilian pulmonary mesenchyme that correlates with extensive innervation and spontaneous smooth muscle contraction, far exceeding that of mammalian or avian lungs at similar stages of development.

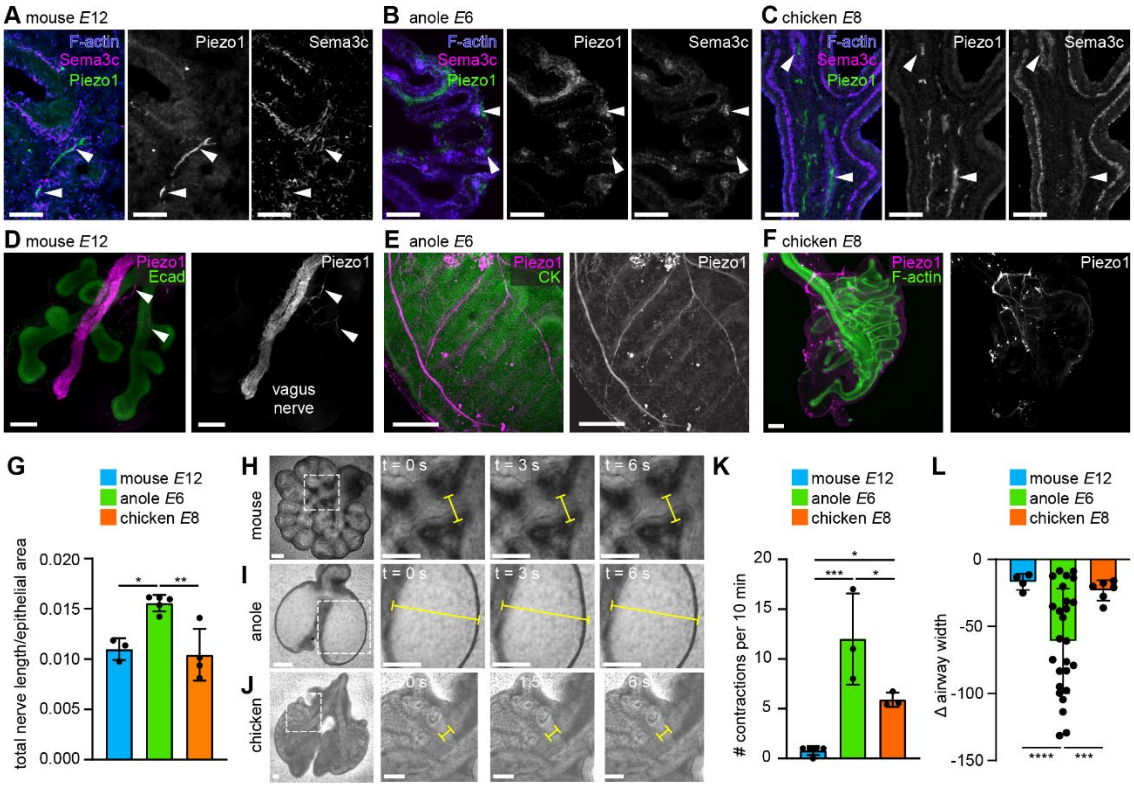

Figure 5: Differences in Sema3c$^+$ mesenchymal cells may support different levels of innervation in each species. (**A-C**) Sections of *E*12 mouse, *E*6 anole, and *E*8 chicken lungs immunostained for Sema3c, Piezo1, and F-actin. Arrowheads indicate Sema3c$^+$ mesenchyme around Piezo1$^+$ neurons. Scale bars indicate 50 µm. (**D-F**) *E*12 mouse, *E*6 anole, and *E*8 chicken lungs immunostained for Piezo1 and either Ecad, CK, or F-actin. Vagus nerve running along mouse lung is indicated. Arrowheads indicate sparse nerves in mouse lung. Scale bars indicate 50 µm. (**G**) Extent of innervation quantified as total length of all Piezo1$^+$ nerves normalized to epithelial area and compared using one-way ANOVA. (**H-J**) *E*12 mouse, *E*6 anole, and *E*8 chicken lungs cultured at an air-liquid interface and imaged every 3 seconds to visualize spontaneous contractions. Yellow line shows width of airway before, during, and after contractions. Scale bars indicate 100 µm. (**K**) Number of contractions per 10 minutes compared using one-way ANOVA. (**L**) Change in airway width during contractions compared using one-way Brown-Forsythe and Welch ANOVA. * indicates $p < 0.05$, ** $p < 0.01$, *** $p<0.001$, **** $p<0.0001$.

Discussion

Using scRNA-seq, comparative immunofluorescence analysis, and *ex vivo* manipulations, we identify species-specific attributes of the pulmonary mesenchyme in terrestrial vertebrates. During early stages of lung development, the mesenchyme of mouse and anole but not chicken lungs appears primed to bind to Shh secreted from the epithelium, which drives airway smooth muscle differentiation and epithelial morphogenesis. In contrast, the mesenchyme of the embryonic chicken lung neither expresses receptors for Shh nor differentiates into smooth muscle at these stages of development. *In situ* hybridization analysis of the early chicken lung shows a thin, spatially restricted domain of *Ptch1* and *Hhip* in the mesenchyme immediately adjacent to the *Shh*-expressing epithelium[33]. Our data suggest that either the

cells of this domain constitute only a small part of the pulmonary mesenchyme or that the expression of these genes is very low. Either scenario could explain why *Ptch1* and *Hhip* expression levels do not drive clustering in our transcriptomic dataset. Ectopically inducing Shh signaling in chicken lungs leads to surprising patterns of expression of smooth muscle markers by the mesothelium and subsequent invasion into the distal mesenchyme. Based on its location and timing, we hypothesize that this mesothelially-derived population of αSMA-expressing cells later wraps and influences the morphogenesis of the distal air sacs. Similar transdifferentiation events have been reported in the morphogenesis of other systems. In the chicken, coronary smooth muscle is derived from cells of the epicardium (which shares its origin with the pulmonary mesothelium) that invade the embryonic heart[34,35]. In the mouse, epicardial cells contribute to the cardiomyocyte lineage of the embryonic heart[36,37] and mesothelial cells contribute to vascular smooth muscle in the lung[38] and gut[39]. Airway smooth muscle of the mouse lung has also been proposed to be derived (if only to a very minor extent) from the mesothelium[40,41]. Additional work is required to precisely distinguish the origins and transcriptional signatures of the air-sac smooth muscle in the chicken lung.

Whereas mouse and anole pulmonary smooth muscle are transcriptionally similar to airway smooth muscle from published datasets, chicken airway smooth muscle resembles, and may originate from, vascular smooth muscle. The divergence in the smooth muscle gene-expression program between species could be related to the fact that both the mouse and the anole require smooth muscle early in lung development to facilitate epithelial morphogenesis[8,9,11]. In the absence of smooth muscle progenitors in the pulmonary mesenchyme around branch tips, suggested by a paucity of *Ptch1* expression in the chicken lung (**Fig. 1F**), airway smooth muscle may then need to come from an external source, such as vascular smooth muscle, as our findings suggest. We are unaware of any other examples of vascular smooth muscle contributing to airway or visceral smooth muscle. If all (or even a significant portion of) airway smooth muscle in the chicken embryo derives from migrating vascular smooth muscle cells, this would constitute a new cellular mechanism for populating a developing organ with visceral smooth muscle.

Using integrated analysis of our scRNA-seq datasets, we also identified species-specific differences in the mesenchyme, including a bias for proliferative mesenchymal cells in mouse and a mesenchymal population enriched in the anole. Intriguingly, we found that the cluster of mesenchymal cells enriched in the anole may promote nerve growth, correlating with the dramatically higher levels of innervation and smooth muscle contraction at the early stages of development of the reptilian lung. We previously found that smooth muscle contraction is not required for epithelial morphogenesis in the developing anole lung[11]. However, it has been suggested that smooth muscle helps to maintain structural integrity and prevent collapse of reptilian lungs[7]. In contrast, mammals and birds rely on surfactant-regulated surface tension and epithelial stiffness to maintain the patency of their far narrower airways[4,42,43]. Furthermore, smooth muscle innervation and contraction at early stages of development might promote maturation of the anole lung prior to hatching. Finally, smooth muscle contraction acts as the primary mechanism for exhalation in many amphibians[7], and while lizards are known to primarily use locomotive muscles for breathing[44] (in contrast to birds and mammals, which have muscles that are used only for breathing[4,45]), a contractile smooth muscle meshwork could represent the retention of an ancestral trait that provides a secondary mechanism for exhalation. Indeed, using locomotive musculature for ventilation limits the ability of certain reptiles to breathe while running[44]. These observations suggest that a fully developed

smooth muscle meshwork, strengthened by contractions during embryogenesis, could imbue a small survival advantage to lizards after hatching.

Collectively, these data shed new light on a variety of morphogenetic motifs that differ in pattern and timing between groups of terrestrial vertebrates. These morphogenetic variations underlie the dramatic differences in final lung architecture and physiology observed across these clades. Our observations also highlight how a handful of conserved mechanisms, altered only in a few parameters such as timing and pattern, can yield divergent, yet still functional, structures. This concept has broad implications for our understanding of the evolution of vertebrate organogenesis.

Acknowledgements
This work was supported in part by the NIH (HD099030, HL164861), the NSF (CMMI-1435853), the Eric and Wendy Schmidt Transformative Technology Fund, and a Faculty Scholars Award from the Howard Hughes Medical Institute. K.G. was supported in part by a postgraduate scholarship-doctoral (PGS-D) from the Natural Sciences and Engineering Research Council of Canada, the Dr. Margaret McWilliams Predoctoral Fellowship from the Canadian Federation of University Women, the Princeton University Procter Fellowship, and an American Heart Association Predoctoral Fellowship. We thank Dr. Wei Wang and the Genomics Core Facility of Princeton University for assistance with transcriptomics.

Author contributions
K.G., M.A.P., and C.M.N. conceptualized the study, designed the experiments, interpreted the data, and wrote the manuscript. K.G., M.A.P., and B.L. performed the experiments and collected the data. All authors provided input on the final manuscript.

Declaration of interests
The authors declare no competing interests.

References

1. Hsia, C.C., Schmitz, A., Lambertz, M., Perry, S.F., and Maina, J.N. (2013). Evolution of air breathing: oxygen homeostasis and the transitions from water to land and sky. Compr Physiol *3*, 849-915. 10.1002/cphy.c120003.

2. Metzger, R.J., Klein, O.D., Martin, G.R., and Krasnow, M.A. (2008). The branching programme of mouse lung development. Nature *453*, 745-750. 10.1038/nature07005.

3. Perry, S.F. (1983). Reptilian lungs. Functional anatomy and evolution. Adv Anat Embryol Cell Biol *79*, 1-81.

4. Maina, J.N. (2005). The Lung-Air Sac System of Birds: Development, Structure, and Function (Springer).

5. Shyer, A.E., Tallinen, T., Nerurkar, N.L., Wei, Z., Gil, E.S., Kaplan, D.L., Tabin, C.J., and Mahadevan, L. (2013). Villification: how the gut gets its villi. Science *342*, 212-218. 10.1126/science.1238842.

6. Walton, K.D., Kolterud, A., Czerwinski, M.J., Bell, M.J., Prakash, A., Kushwaha, J., Grosse, A.S., Schnell, S., and Gumucio, D.L. (2012). Hedgehog-responsive mesenchymal clusters direct patterning and emergence of intestinal villi. Proc Natl Acad Sci U S A *109*, 15817-15822. 10.1073/pnas.1205669109.

7. Cieri, R.L. (2019). Pulmonary Smooth Muscle in Vertebrates: A Comparative Review of Structure and Function. Integr Comp Biol *59*, 10-28. 10.1093/icb/icz002.

8. Goodwin, K., Mao, S., Guyomar, T., Miller, E., Radisky, D.C., Kosmrlj, A., and Nelson, C.M. (2019). Smooth muscle differentiation shapes domain branches during mouse lung development. Development *146*. 10.1242/dev.181172.

9. Kim, H.Y., Pang, M.F., Varner, V.D., Kojima, L., Miller, E., Radisky, D.C., and Nelson, C.M. (2015). Localized Smooth Muscle Differentiation Is Essential for Epithelial Bifurcation during Branching Morphogenesis of the Mammalian Lung. Dev Cell *34*, 719-726. 10.1016/j.devcel.2015.08.012.

10. Jesudason, E.C. (2007). Exploiting mechanical stimuli to rescue growth of the hypoplastic lung. Pediatr Surg Int *23*, 827-836. 10.1007/s00383-007-1956-0.

11. Palmer, M.A., Nerger, B.A., Goodwin, K., Sudhakar, A., Lemke, S.B., Ravindran, P.T., Toettcher, J.E., Kosmrlj, A., and Nelson, C.M. (2021). Stress ball morphogenesis: How the lizard builds its lung. Sci Adv *7*, eabk0161. 10.1126/sciadv.abk0161.

12. Rose, C.S., and James, B. (2013). Plasticity of lung development in the amphibian, Xenopus laevis. Biol Open *2*, 1324-1335. 10.1242/bio.20133772.

13. Kim, H.Y., Varner, V.D., and Nelson, C.M. (2013). Apical constriction initiates new bud formation during monopodial branching of the embryonic chicken lung. Development *140*, 3146-3155. 10.1242/dev.093682.

14. Spurlin, J.W., Siedlik, M.J., Nerger, B.A., Pang, M.F., Jayaraman, S., Zhang, R., and Nelson, C.M. (2019). Mesenchymal proteases and tissue fluidity remodel the extracellular matrix during airway epithelial branching in the embryonic avian lung. Development *146*. 10.1242/dev.175257.

15. Tzou, D., W. Spurlin J, r., Pavlovich, A.L., Stewart, C.R., Gleghorn, J.P., and Nelson, C.M. (2016). Morphogenesis and morphometric scaling of lung airway development follows phylogeny in chicken, quail, and duck embryos. Evodevo *7*, 12. 10.1186/s13227-016-0049-3.

16. Palmer, M.A., and Nelson, C.M. (2020). Fusion of airways during avian lung development constitutes a novel mechanism for the formation of continuous lumena in multicellular epithelia. Dev Dyn *249*, 1318-1333. 10.1002/dvdy.215.

17. Goodwin, K., Jaslove, J.M., Tao, H., Zhu, M., Hopyan, S., and Nelson, C.M. (2022). Patterning the embryonic pulmonary mesenchyme. iScience *25*, 103838. 10.1016/j.isci.2022.103838.

18. Brunskill, E.W., Park, J.S., Chung, E., Chen, F., Magella, B., and Potter, S.S. (2014). Single cell dissection of early kidney development: multilineage priming. Development *141*, 3093-3101. 10.1242/dev.110601.

19. Pepicelli, C.V., Lewis, P.M., and McMahon, A.P. (1998). Sonic hedgehog regulates branching morphogenesis in the mammalian lung. Curr Biol *8*, 1083-1086. 10.1016/s0960-9822(98)70446-4.

20. Jones, M.R., Chong, L., and Bellusci, S. (2020). Fgf10/Fgfr2b Signaling Orchestrates the Symphony of Molecular, Cellular, and Physical Processes Required for Harmonious Airway Branching Morphogenesis. Front Cell Dev Biol *8*, 620667. 10.3389/fcell.2020.620667.

21. Abler, L.L., Mansour, S.L., and Sun, X. (2009). Conditional gene inactivation reveals roles for Fgf10 and Fgfr2 in establishing a normal pattern of epithelial branching in the mouse lung. Dev Dyn *238*, 1999-2013. 10.1002/dvdy.22032.

22. Moura, R.S., Coutinho-Borges, J.P., Pacheco, A.P., Damota, P.O., and Correia-Pinto, J. (2011). FGF signaling pathway in the developing chick lung: expression and inhibition studies. PLoS One *6*, e17660. 10.1371/journal.pone.0017660.

23. Danopoulos, S., Thornton, M.E., Grubbs, B.H., Frey, M.R., Warburton, D., Bellusci, S., and Al Alam, D. (2019). Discordant roles for FGF ligands in lung branching morphogenesis between human and mouse. J Pathol *247*, 254-265. 10.1002/path.5188.

24. Stanton, B.Z., and Peng, L.F. (2010). Small-molecule modulators of the Sonic Hedgehog signaling pathway. Mol Biosyst *6*, 44-54. 10.1039/b910196a.

25. Zepp, J.A., Morley, M.P., Loebel, C., Kremp, M.M., Chaudhry, F.N., Basil, M.C., Leach, J.P., Liberti, D.C., Niethamer, T.K., Ying, Y., et al. (2021). Genomic, epigenomic, and biophysical cues controlling the emergence of the lung alveolus. Science *371*. 10.1126/science.abc3172.

26. de Soysa, T.Y., Ranade, S.S., Okawa, S., Ravichandran, S., Huang, Y., Salunga, H.T., Schricker, A., Del Sol, A., Gifford, C.A., and Srivastava, D. (2019). Single-cell analysis of cardiogenesis reveals basis for organ-level developmental defects. Nature *572*, 120-124. 10.1038/s41586-019-1414-x.

27. Rodda, L.B., Lu, E., Bennett, M.L., Sokol, C.L., Wang, X., Luther, S.A., Barres, B.A., Luster, A.D., Ye, C.J., and Cyster, J.G. (2018). Single-Cell RNA Sequencing of Lymph Node Stromal Cells Reveals Niche-Associated Heterogeneity. Immunity *48*, 1014-1028 e1016. 10.1016/j.immuni.2018.04.006.

28. Rubenstein, A.B., Smith, G.R., Raue, U., Begue, G., Minchev, K., Ruf-Zamojski, F., Nair, V.D., Wang, X., Zhou, L., Zaslavsky, E., et al. (2020). Single-cell transcriptional profiles in human skeletal muscle. Sci Rep *10*, 229. 10.1038/s41598-019-57110-6.

29. Hasleton, P. (1996). Spencer's pathology of the lung. Anatomy of the lung. Hasleton PS and Curry A (edrs) *1*, 6-7.

30. Mennega, A. (1964). The Tracheal Rings in Domestic Birds. Poultry Science *43*, 1279. https://doi.org/10.3382/ps.0431279.

31. Den Hondt, M., and Vranckx, J.J. (2017). Reconstruction of defects of the trachea. J Mater Sci Mater Med *28*, 24. 10.1007/s10856-016-5835-x.

32. Klingler, J.J. (2016). On the Morphological Description of Tracheal and Esophageal Displacement and Its Phylogenetic Distribution in Avialae. PLoS One *11*, e0163348. 10.1371/journal.pone.0163348.

33. Moura, R.S., Silva-Goncalves, C., Vaz-Cunha, P., and Correia-Pinto, J. (2016). Expression analysis of Shh signaling members in early stages of chick lung development. Histochem Cell Biol *146*, 457-466. 10.1007/s00418-016-1448-1.

34. Mikawa, T., and Gourdie, R.G. (1996). Pericardial mesoderm generates a population of coronary smooth muscle cells migrating into the heart along with ingrowth of the epicardial organ. Dev Biol *174*, 221-232. 10.1006/dbio.1996.0068.

35. Dettman, R.W., Denetclaw, W., Jr., Ordahl, C.P., and Bristow, J. (1998). Common epicardial origin of coronary vascular smooth muscle, perivascular fibroblasts, and intermyocardial fibroblasts in the avian heart. Dev Biol *193*, 169-181. 10.1006/dbio.1997.8801.

36. Zhou, B., Ma, Q., Rajagopal, S., Wu, S.M., Domian, I., Rivera-Feliciano, J., Jiang, D., von Gise, A., Ikeda, S., Chien, K.R., and Pu, W.T. (2008). Epicardial progenitors contribute to the cardiomyocyte lineage in the developing heart. Nature *454*, 109-113. 10.1038/nature07060.

37. Cai, C.L., Martin, J.C., Sun, Y., Cui, L., Wang, L., Ouyang, K., Yang, L., Bu, L., Liang, X., Zhang, X., et al. (2008). A myocardial lineage derives from Tbx18 epicardial cells. Nature *454*, 104-108. 10.1038/nature06969.

38. Que, J., Wilm, B., Hasegawa, H., Wang, F., Bader, D., and Hogan, B.L. (2008). Mesothelium contributes to vascular smooth muscle and mesenchyme during lung development. Proc Natl Acad Sci U S A *105*, 16626-16630. 10.1073/pnas.0808649105.

39. Wilm, B., Ipenberg, A., Hastie, N.D., Burch, J.B., and Bader, D.M. (2005). The serosal mesothelium is a major source of smooth muscle cells of the gut vasculature. Development *132*, 5317-5328. 10.1242/dev.02141.

40. Dixit, R., Ai, X., and Fine, A. (2013). Derivation of lung mesenchymal lineages from the fetal mesothelium requires hedgehog signaling for mesothelial cell entry. Development *140*, 4398-4406. 10.1242/dev.098079.

41. Moiseenko, A., Kheirollahi, V., Chao, C.M., Ahmadvand, N., Quantius, J., Wilhelm, J., Herold, S., Ahlbrecht, K., Morty, R.E., Rizvanov, A.A., et al. (2017). Origin and characterization of alpha smooth muscle actin-positive cells during murine lung development. Stem Cells *35*, 1566-1578. 10.1002/stem.2615.

42. Bernhard, W., Gebert, A., Vieten, G., Rau, G.A., Hohlfeld, J.M., Postle, A.D., and Freihorst, J. (2001). Pulmonary surfactant in birds: coping with surface tension in a tubular lung. Am J Physiol Regul Integr Comp Physiol *281*, R327-337. 10.1152/ajpregu.2001.281.1.R327.

43. Enhorning, G. (1996). Pulmonary Surfactant Function in Alveoli and Conducting Airways. Canadian Respiratory Journal *3*, 364751. 10.1155/1996/364751.

44. Wang, T., Carrier, D.R., and Hicks, J.W. (1997). Ventilation and gas exchange in lizards during treadmill exercise. J Exp Biol *200*, 2629-2639. 10.1242/jeb.200.20.2629.

45. Fogarty, M.J., and Sieck, G.C. (2019). Evolution and Functional Differentiation of the Diaphragm Muscle of Mammals. Compr Physiol *9*, 715-766. 10.1002/cphy.c180012.

46. Butler, A., Hoffman, P., Smibert, P., Papalexi, E., and Satija, R. (2018). Integrating single-cell transcriptomic data across different conditions, technologies, and species. Nat Biotechnol *36*, 411-420. 10.1038/nbt.4096.

47. Yu, G., Wang, L.G., Han, Y., and He, Q.Y. (2012). clusterProfiler: an R package for comparing biological themes among gene clusters. OMICS *16*, 284-287. 10.1089/omi.2011.0118.

STAR Methods

RESOURCE AVAILABILITY

Lead Contact

- Further information and requests for resources and reagents should be directed to and will be fulfilled by the lead contact, Celeste M. Nelson (celesten@princeton.edu).

Materials availability

- This study did not generate new unique reagents.

Data and code availability

- Single-cell RNA-seq data have been deposited at GEO and are publicly available as of the date of publication. Accession numbers are listed in the key resources table.
- Any additional information required to reanalyze the data reported in this paper is available from the lead contact upon request.

EXPERIMENTAL MODEL AND SUBJECT DETAILS

Animal care and isolation of embryonic lungs

Breeding of CD1 mice and isolation of embryos were carried out in accordance with institutional guidelines following the NIH Guide for the Care and Use of Laboratory Animals and approved by Princeton's Institutional Animal Care and Use Committee. Lungs isolated at *E*12.5 were dissected with forceps in sterile PBS and the left lobe was further isolated from each lung using tungsten needles (Fine Science Tools). Wild-caught brown anoles (*Anolis sagrei*) were obtained through a commercial vendor and maintained in a temperature-, humidity-, and light-controlled environment at a ratio of 1 male to 3 females. Tanks were inspected daily and eggs were collected and incubated in a benchtop incubator at 30°C and 80% humidity until the desired stage. Embryos were dissected with forceps under a microscope to isolate the lungs and trachea. Fertilized chicken (*Gallus gallus* variant *domesticus*) eggs were obtained from Moyer's chicks (Quakertown, PA) and incubated at 38°C in a humidified chamber until the desired stage. Embryos were dissected with forceps under a microscope to isolate the lungs.

METHOD DETAILS

scRNA-seq experiments

Lungs were isolated from embryos at the stages of interest and then dissociated with dispase at room temperature for 10 minutes, with additional mechanical dissociation using fine tungsten needles to generate single-cell suspensions. Dispase was inactivated by adding DMEM/F12 medium (without HEPES) supplemented with 5% heat-inactivated fetal bovine serum (FBS; Atlanta Biologicals) and antibiotics (50 units/ml of penicillin and streptomycin) and the cell suspensions were then passed through 40-µm-diameter mesh filters. scRNA-seq libraries were prepared and sequenced by the Princeton Genomics Core Facility. Cells were loaded and processed using the Chromium Single Cell 3' Library and Gel Bead Kit v3 on the Chromium Controller (10X Genomics) following manufacturer protocols. Individual cells were encapsulated in droplets with individual gel beads carrying unique barcoded primers and lysed. Then, cDNA fragments were synthesized, barcoded, and amplified by PCR. Illumina sequencing libraries were prepared from the amplified cDNA from each sample group using the Nextra

DNA library prep kit (Illumina). Libraries were sequenced on NovaSeq 6000 S Prime flowcells (Illumina) as paired-end 28 + 94 nucleotide reads, following manufacturer protocols. Base calling was performed and raw sequencing reads were filtered using the Illumina sequencer control software to keep only pass-filtered reads for downstream analysis. The 10x CellRanger software version 3.0.2 was used to run the count pipeline with default settings on all FASTQ files from each sample to generate gene-barcode matrices using the *Mus musculus* reference genome mm10-1.2.0, the *Anolis carolinensis* reference genome AnoCar2.0, or the *Gallus gallus* reference genome GRCg6a. The mouse and chicken datasets are available on GEO (GSE203212). The anole datasets are previously published (GSE171416).

Immunofluorescence analysis

Lungs were fixed in 4% paraformaldehyde in PBS for either 15 minutes at room temperature or 30 minutes at 4°C and then permeabilized with 0.1% Triton X-100 in PBS. Prior to staining, lungs were blocked with 0.1% BSA and 5% goat serum in PBS with 0.1% Triton X-100. Lungs were then incubated overnight with primary antibodies against αSMA (Sigma a5228, 1:400 or Abcam ab5694, 1:200), CD31 (Abcam ab28364, 1:200), epithelial cytokeratins (CK; Dako Z0622, 1:400), E-cadherin (Invitrogen 13-1900, 1:200), LCAM (DHSB 7D6, 1:50), Piezo1 (Invitrogen PA5-77617, 1:200), Sema3c (R&D Systems MAB1728, 1:200), and/or Sox9 (Abcam ab26414, 1:1000) diluted in blocking buffer, followed by incubation with Alexa Fluor-conjugated secondary antibodies (1:200) or phalloidin (1:400) and Hoechst (1:1000). Lungs were then dehydrated in a methanol (or isopropanol for phalloidin-stained samples) series and then cleared in Murray's Clear (1:2 benzyl alcohol:benzyl benzoate) or cleared without dehydration in serial dilutions of glycerol (25, 50, 75, and 100%). Lung sections were mounted in Fluoromount (Thermo Fisher). Lungs were imaged on an inverted spinning-disk confocal microscope (Nikon Ti equipped with X-light) using 20× objectives (0.45 *NA* or 0.7 *NA*). EdU incorporation assays were carried out on explanted lungs after one hour of acclimation in culture. EdU was added to the culture medium for 30 minutes prior to fixation (Click-iT EdU Kit, Thermo Fisher C10338).

***Ex vivo* culture**

Lungs were isolated from mouse, anole, or chicken embryos at the indicated stages and cultured at an air-liquid interface atop porous filters floating on DMEM/F12 medium (without HEPES) supplemented with 5% heat-inactivated fetal bovine serum (FBS; Atlanta Biologicals) and antibiotics (50 units/ml of penicillin and streptomycin). Explants were incubated for 24 hours at 37ºC under 5% CO_2. For DiI experiments, lungs were submerged in PBS with 5% Vybrant DiI cell labeling solution (Invitrogen V22885) for 20 minutes at 37ºC. To activate Shh signaling, the culture medium was supplemented with 1 µg/ml smoothened agonist (SAG; Calbiochem).

QUANTIFICATION AND STATISTICAL ANALYSES

scRNA-seq data analysis

scRNA-seq data were exported from Cell Ranger and then imported into R. The data were then processed using the Seurat package[46]. Datasets were normalized and integrated using the Seurat function FindVariableFeatures based on 2000 genes. The datasets were then scaled before analysis using the Seurat functions FindNeighbors and FindClusters to find neighbors and clusters. Finally, we visualized clusters using the uniform manifold approximation and projection (UMAP) dimensional reduction. Initial

clustering was carried out on all cells, and then mesenchymal and smooth muscle cell clusters were computationally isolated for further analysis.

For Pearson correlation analysis, we first downloaded from GEO eight published scRNA-seq datasets, representing embryonic and postnatal mouse lungs (GSE149563, GSE149563, GSE149563, and GSE149563), embryonic mouse hearts isolated at *E*7.75, *E*8.25, and *E*9.25 (GSE126128), lymph node stromal cells from adult mice (GSE112903), and quadricep and diaphragm skeletal muscle from adult mice (GSE138707). All datasets were processed following the standard Seurat pipeline and relevant clusters were identified based on markers used in the original publications (**Fig. S3**). In the lung datasets, we used *Acta2* with *Hhip* for airway smooth muscle, *Acta2* with *Notch3* for vascular smooth muscle, *Acta2* with *Stc1* for myofibroblasts, and *Acta2* with *Pdgfrb* for pericytes[25]. In the heart dataset, we used *Acta2*, *Myl9*, and *Ttn* to identify myocardial cells[26]. In the lymph node stromal cell dataset, we used *Acta2*, *Myh11*, and *Myl9* to identify lymphatic smooth muscle cells[27]. In the skeletal muscle datasets, which contained only mononucleated cells, we used *Myod1* and *Pax7* to identify muscle stem cells[28]. For each dataset, we then obtained average expression values of variable genes (based on the Seurat pipeline) for the cluster(s) of interest. We then filtered these lists based on whether genes were also detected in smooth muscle cells of our datasets, and then chose the top 50 markers per list based on highest expression level. Finally, we performed Pearson correlation analysis using these top 50 markers for each of our smooth muscle cell clusters (mouse *E*12 – cluster 4, anole *E*6 – cluster 1, and chicken *E*8 – cluster 1).

For the integrated analysis, we used the Seurat tools to find integration anchors and perform integration of three datasets: mouse *E*12, anole *E*6, and chicken *E*8. The integrated dataset was then processed to obtain clusters and UMAPs. Gene ontology analysis was performed on markers for each cluster using the clusterProfiler package in R[47].

Image analysis and statistics

Images were analyzed using Fiji. Position and width of αSMA-expressing or DiI-labeled cells in cultured lungs were measured manually and then compared using ANOVA. Percent of EdU^+ cells was measured by manually counting the number of EdU^+ cells and total number of cells (based on Hoechst stain) in three 100 × 100-pixel windows per lung. The mean of these three windows per lung was calculated and groups were compared using ANOVA.

Supplementary Movies

Supplementary Movie 1. Time-lapse imaging of explanted *E*12 mouse lungs in culture showing spontaneous contractions of the airways.

Supplementary Movie 2. Time-lapse imaging of explanted *E*6 anole lungs in culture showing spontaneous contractions of the airways.

Supplementary Movie 3. Time-lapse imaging of explanted *E*8 chicken lungs in culture showing spontaneous contractions of the airways.

Supplementary Figures

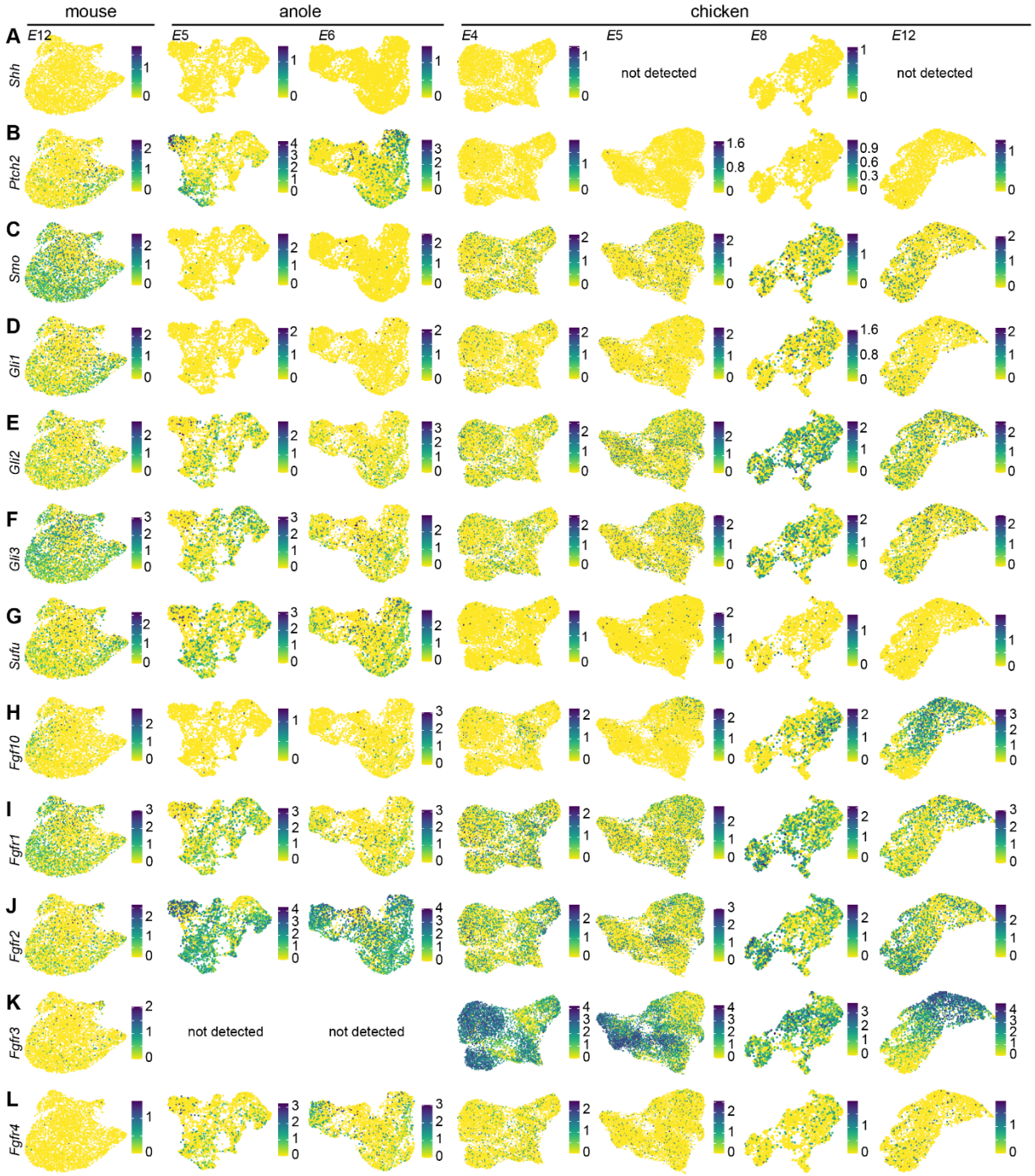

Supplementary Figure 1 – related to Figure 1. Expression of Shh-pathway components, *Fgf10*, and FGFR genes across species. UMAPs from **Fig. 1D** color-coded by expression of *Shh*, *Ptch2*, *Smo*, *Gli1*, *Gli2*, *Gli3*, *Sufu*, *Fgf10*, *Fgfr1*, *Fgfr2*, *Fgfr3*, and *Fgfr4*.

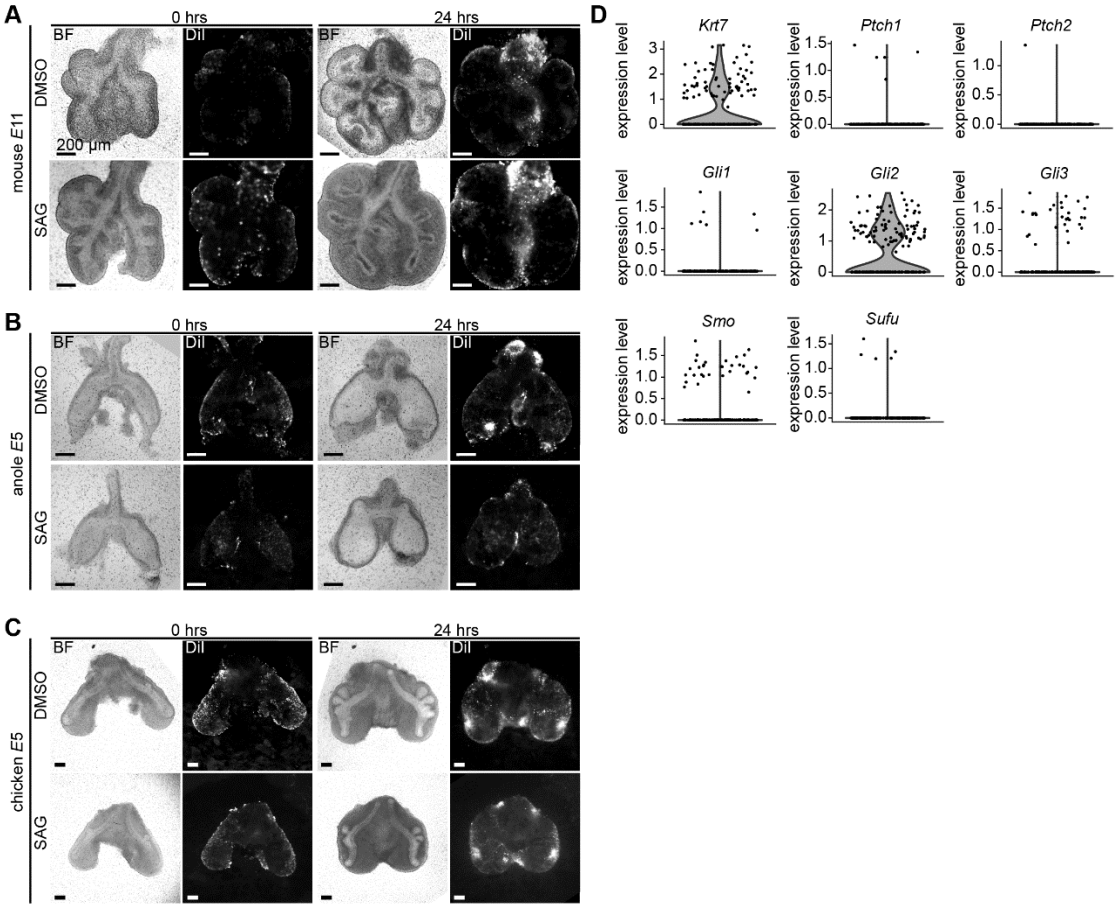

Supplementary Figure 2 – related to Figure 2. (**A-C**) Brightfield and fluorescence images of mouse lungs isolated at *E*11, anole lungs isolated at *E*5, or chicken lungs isolated at *E*5, incubated with DiI to label the mesothelial surface, and then cultured for 24 hours *ex vivo* in the presence of DMSO or SAG (1 µg/ml). (**D**) Expression levels of the mesothelial marker keratin 7 (*Krt7*) and of Shh-pathway components *Ptch1*, *Ptch2*, *Gli1*, *Gli2*, *Gli3*, *Smo*, and *Sufu* in mesothelial cells in the scRNA-seq dataset generated from *E*5 chicken lungs.

Supplementary Figure 3 – related to Figure 3. UMAPs color-coded by cluster and by the expression of genes used to identify populations of interest for the datasets subjected to Pearson correlation analysis in **Fig. 3A-C**. (**A-D**) Airway smooth muscle (ASM), vascular smooth muscle (VSM), myofibroblasts, and pericytes were identified from datasets generated at four stages of mouse lung development (GSE149563, GSE149563, GSE149563, and GSE149563)[25]. (**E**) Myocardial cells were identified as 5 clusters from a dataset of embryonic mouse hearts isolated at *E*7.75, *E*8.25, and *E*9.25 (GSE126128)[26]. (**F**) Lymphatic smooth muscle cells were identified from a dataset of lymph node stromal cells from adult mice (GSE112903)[27]. (**G-H**) Muscle stem cells were identified from datasets generated from adult mouse quadricep or diaphragm skeletal muscle (GSE138707)[28].